Fire Safety Journal 91 (2017) 776–783

Contents lists available at ScienceDirect

Fire Safety Journal

journal homepage: www.elsevier.com/locate/firesaf

IAFSS 12th Symposium 2017

Verification of a Lagrangian particle model for short-range firebrand transport

Rahul Wadhwani[a,b,*], Duncan Sutherland[a,b,c], Andrew Ooi[b,c], Khalid Moinuddin[a,b], Graham Thorpe[b,d]

[a] Centre for Environmental Safety and Risk Engineering, Victoria University, Melbourne, VIC 3030, Australia
[b] Bushfire and Natural Hazards CRC, Melbourne, VIC 3002, Australia
[c] Department of Mechanical Engineering, University of Melbourne, Melbourne, VIC 3052, Australia
[d] College of Engineering and Science, Victoria University, Melbourne, VIC 3011, Australia

ARTICLE INFO

Keywords:
Short-range firebrands
Lagrangian particles
Fire Dynamics Simulator (FDS)

ABSTRACT

Firebrands are a harbinger of damage to infrastructure; their effects cause a particularly important threat to people living within the wildland-urban-interface. Short-range firebrands travel with the wind with little or no lofting, and cause spotfires. In this work, the design of a novel firebrand generator prototype is discussed to achieve a uniform shower of firebrands. The transport of short-range firebrand is studied to verify the existing Lagrangian particle model of Fire Dynamics Simulator. Uniform, non-combusting cubiform and cylindrical firebrands are projected using the firebrand generator. The experimentally observed distribution of particles on the ground is compared with a simulated distribution using the fire dynamic simulator. The results show that the existing Lagrangian model gives a good agreement with the experimental data.

1. Introduction

Wildfires are a frequent occurrence in Australia, and they can severely impact the economy e.g. the Black Saturday fire 2009 [1]. Other countries such as the United States, Spain, and Portugal also suffer from the economic and human losses from wildfires [2]. The majority of the economic and human life losses occur for the society who are living on the wildland-urban-interface (WUI) [3]. To predict how wildfires spread many mathematical models have been developed based on theoretical studies, experimental work, and computational data [4–6]. Firebrands (which are burning pieces of bark, twigs, leaves and nuts) play a major role in causing damage to the infrastructures located on the WUI [4,7,8] and seed the propagation of wildfires [4–6,8] by creating spotfires. The spotting phenomena of these firebrands are classified based on the distance that the firebrand travels: (a) short-range (500–750 m), (b) medium-range (1000–1500 m), and (c) long-range spotting (> 5000 m) [9].

Long-range spotting is the result of significant lofting of firebrands by the wind and plume during a wildfire causing firebrand to travel distances from a few kilometres to tens of kilometres [8,9]. These firebrands are typically generated at the upper layer of the forest canopy due to a crown fire and transported by the wind blowing near the canopy surface. Transport and spotfires ignited by these types of firebrands have been studied extensively [9–12]. However, information on short-range spotting is somewhat exiguous [9]. Short-range spotting is the outcome of firebrands blown away by the wind from the fire front location with little or no lofting. The short-range firebrands have flatter trajectories and are generated from the mid-/lower-upper- section of the forest. The spotting density of this type of firebrands decreases with the distance away from the fire front. These firebrands maintain the propagation of fires over fuel surfaces or damage infrastructure located at the somewhat heterogeneous WUI [7]. There is very little understanding on how short-range spotfire coalesce with the fire front and the distribution density of the firebrand from the fire front [9].

The transport of firebrands usually depends on the characteristic features of firebrands such as shape, size, mass, original height (the point of generation), and wind speed [13,14]. A firebrand generator can be used to artificially create a firebrand shower to study the aerodynamics and the impact of firebrands on the infrastructure, or a fuel bed. The NIST Firebrand dragon [2,15], designed and constructed by the National Institute of Standards and Technologies (NIST), USA, is the one such firebrand generator that has been used extensively to explore the vulnerabilities of structures exposed to firebrand showers [16–18]. However, we suspect that the flow within the NIST Firebrand dragon will be reasonably complex and difficult to use for conducting benchmark experiments to develop and validate a model for short-

* Corresponding author at: Centre for Environmental Safety and Risk Engineering, Victoria University, Melbourne, VIC 3030, Australia.
E-mail address: rahul.wadhwani@live.vu.edu.au (R. Wadhwani).

http://dx.doi.org/10.1016/j.firesaf.2017.03.019
Received 14 February 2017; Accepted 15 March 2017
Available online 04 May 2017

Nomenclature

$C_{D,\ spherical}$	Drag coefficient for spherical particles
$C_{D,\ cylindrical}$	Drag coefficient for cylindrical particles
d_p	Diameter of pitot tube (mm)
D	Particle characteristic diameter (m)
D_{ID}	Nominal inner diameter of pipe (mm)
$f_i(x,y)$	number of particles in distribution grid x, y
i	Experiment number for particle transport
μ	Dynamic viscosity of air (Pa.s)
$\overline{\mu}$	Mean density of particles
N	Maximum number of experiments carried out for ensemble average
$P_i(x,y)$	Ensemble average of particle distribution after ith experiment in x,y distribution grid
ρ_f	Density of fluid (or air) (kg/m^3)
r^*	Radial distance=Distance from centre of pipe/Radius of pipe
Re	Reynolds number of fluid based on the fluid velocity and pipe radius
Re_D	Particle Reynolds number based on the velocity of the particle relative to the fluid and particle size
σ	Standard deviation of particles density
u'	Average velocity fluctuation measured by the pitot tube (m/s)
u_τ	Friction velocity (m/s)
U	Relative velocity of the particle to the fluid (m/s)
U_{act}	Actual average velocity of flow measured by the pitot tube (m/s)
U_{meas}	Measured average velocity of flow measured by the pitot tube (m/s)
υ	Kinematic viscosity of air (m^2/s)
x_l, x_u	Lower and upper limit of distribution grid in x direction
y_l, y_u	Lower and upper limit of distribution grid in y direction

range firebrand transport. The sharp bend upstream of the mouth of NIST Firebrand dragon generates eddies near the outlet thus creating a non-uniform flow field at the exit of the generator. Therefore, to conduct benchmark experiments for short-range firebrands and to understand their aerodynamics and scattering distribution we constructed a prototype firebrand generator which provides a uniform flow field at the exit (details of the design will be discussed later in this manuscript).

In the last two decades, fire models based on computational fluid dynamics (CFD) methodology are increasingly used to simulate and study engineering problems involving fire. This growth in the use of CFD-based models is due to the increase in computational capabilities. Fire Dynamic Simulator (FDS), developed by NIST, is a widely used open-source CFD based fire model used to study the fire behaviour in infrastructure fire. Mell et al. [19,20] have discussed the applicability of a version of FDS to study grassfire propagation and tree fires. A Lagrangian particle model, one of the sub-models of FDS, has been extensively used, verified and validated for the transport of liquid particles used in sprinkler and nozzle building-fire suppression systems [21–23]. However, use of the Lagrangian model for the transport of

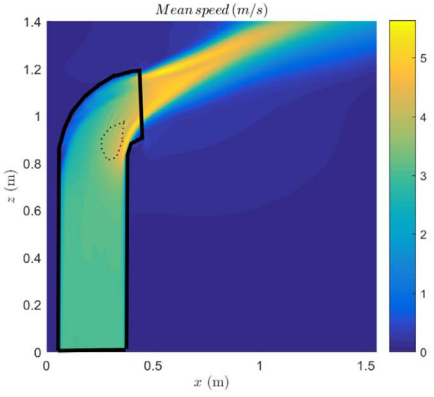

(a) Contours of mean speed in the XZ plane

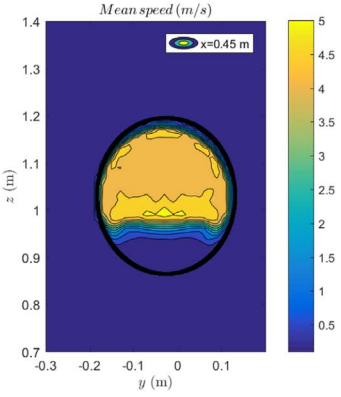

(b) Contours of mean speed in the YZ plane

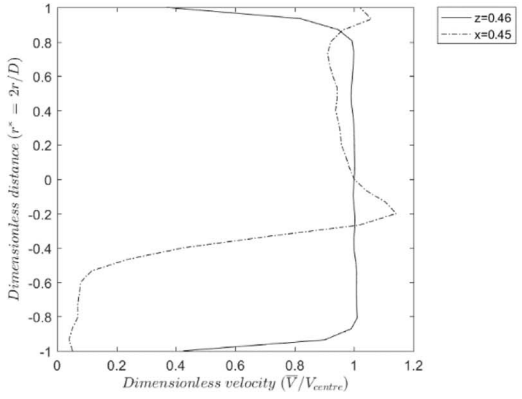

(c) Normalised velocity computed at two locations: inside the tube (z=0.46m), and at the mouth of tube (x=0.45m)

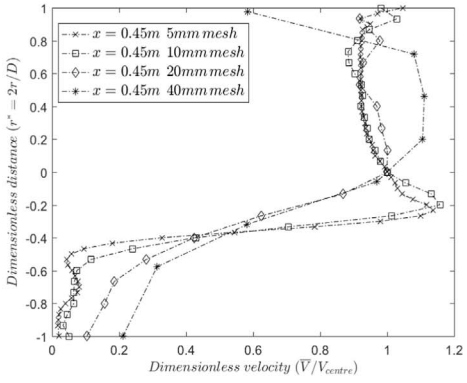

(d) Grid sensitivity for normalised velocity at the mouth of tube (x=0.45m)

Fig. 1. Mean flow profiles at the outlet of the NIST Firebrand dragon.

solid particles is limited. Hence, as a first step, we wish to verify the FDS Lagrangian particle model for the transport of non-burning solid firebrands. The comprehensive modelling of a flaming firebrand is complicated and involves accounting for the combustion, mass loss and self-buoyancy of the particle. These effects are difficult to account for in the first instance. Therefore, the design of firebrand generator prototype and validation study for only non-burning firebrands are presented in this study.

2. Numerical model

CFD simulations were carried out using FDS (version 6.2.0) accompanied by Smokeview (version 6.2.2) for visualisation. The basic governing conservation equations for mass, energy and momentum are solved using a second-order finite difference method. The fluid is assumed to be Newtonian. The details of these equations [24] are beyond the scope of this work and they are available in the FDS technical guide [25]. FDS utilises Large-Eddy Simulation (LES) with a default Deardoff turbulence model to describe the gas phase turbulence and a Lagrangian particle model to describe the solid particle transport.

The particle drag coefficient is defined as a function of local Reynolds number based on the particle diameter and relative fluid velocity. The Particle Reynolds number is defined as $Re_D=\rho_f DU/\mu$, where, D and U are particle characteristic diameter and relative velocity of the particle to the fluid, and ρ_f, μ are fluid density and viscosity. For cubiform and cylindrical particles, the drag coefficients used are described by Eq. (1) (for a representation of a cubiform particle) and Eq. (2) (for the cylinder) [25].

$$C_{D,\ \text{spherical}} = \begin{cases} 24/Re_D\ , & Re_D < 1 \\ 24(0.85 + 0.15Re_D^{0.687})/Re_D, & 1 < Re_D < 1000 \\ 1, & Re_D > 1000 \end{cases} \quad (1)$$

(a) VU Firebrand dragon prototype

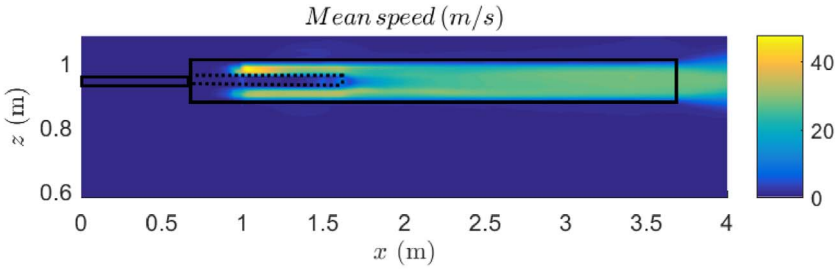

(b) Contours of time averaged speed in the XZ plane

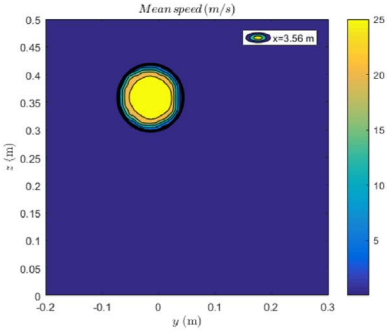

(c) Contours of time averaged speed in the YZ plane

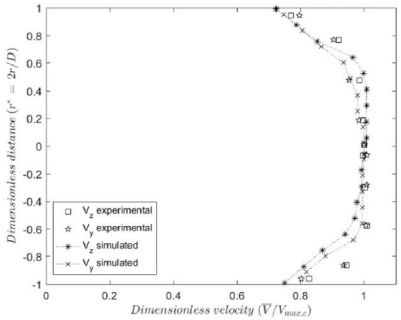

(d) Comparison between experimental and simulated flow profiles

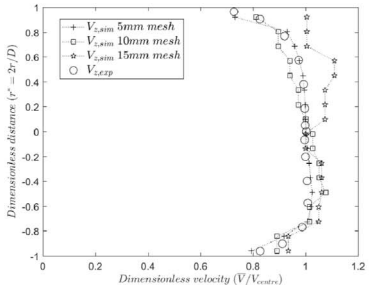

(e) Grid sensitivity for mean flow profile varying along Z-axis with the experimental observation

Fig. 2. VU prototype firebrand generator and mean flow profile observed.

$$C_{D,\text{ cylindrical}} = \begin{cases} 10/Re_D^{0.8}, & Re_D < 1 \\ 10(0.6 + 0.4Re_D^{0.8})/Re_D, & 1 < Re_D < 1000 \\ 1, & Re_D > 1000 \end{cases} \quad (2)$$

Eq. (1) defines the drag coefficient for spherical particles, however, this equation is used for cubiform particles as the sphericity of cubiform particle is 0.806. The assumption is considered valid because the effect of sphericity, and tumbling of particle will be equalised on the distribution grid on ground of 20 cm wide (Refer to Fig. 3).

3. Design of firebrand generator prototype

3.1. Simulation of the NIST dragon

The design of our firebrand generator prototype is based on the flow simulation within the NIST Firebrand dragon [2] in FDS. We reduce the NIST Firebrand dragon to the pipe section [2] only with the uniform inlet velocity at the inlet of the pipe. The simulation of the entire pipe is possible but not computationally feasible as it would require excessive computational resources. We therefore simulate the only the bend of the generator and assume a uniform flow velocity of 3 m/s. The walls of the pipe has no-slip condition while the domain has constant pressure open boundary conditions at x = 0, 1.55 m, y = −0.3, 0.2 m, and z = 0, 1.4 m with a grid size of Δx = Δy = Δz = 10 mm. Fig. 1(a) and (b) shows the time-averaged speed of NIST Firebrand dragon in two planes (X-Z and Y-Z). It can be seen that a Dean's vortex [26] has formed (marked in Fig. 1(a)) near the mouth of the dragon (Reynolds number (Re)≈9700). Fig. 1(c) shows the computed average velocity (normalised with the velocity at the centre of the tube) inside the tube (z = 0.46 m) and at the mouth *(x = 0.45* m) for a 10 mm cubiform mesh grid. Grid sensitivity analysis for cubiform grids of size 5, 10, 20, and 40 mm is carried out and shown in Fig. 1(d). The 10 mm cubiform grid is comparable with the 5 mm cubiform grid size and hence, 10 mm grid is chosen. In Fig. 1(c) we can see that at z = 0.46 m flow profile is largely uniform except near the edges and overall symmetrical about the centre line of the tube. On the other hand, the flow profile at the mouth (x = 0.45 m) is skewed towards the upper edge of the mouth. In this profile, at the lower 20% of the mouth, a very low velocity is observed. A peak velocity is observed near the centre of mouth which is a result of the Dean's vortex formation. Another peak is observed near the upper edge of the tube which is due to the forced flow caused by tube bend. The results obtained for the NIST Firebrand dragon are similar to the CFD simulation of fluid flow obtained for the 90° bent tube [27–30]. Thus, confirming our hypothesis that a non-uniform distribution of firebrands will exist at the mouth of the tube that has a 90° bend immediately upstream of the outlet [27–30]. The sudden change in flow near the mouth also promotes collisions between the firebrands and tube further complicating the computations of the trajectories of the short-range firebrands.

3.2. Design and characterisation of a new prototype firebrand generator

To ensure that the particles leave the firebrand generator in a uniform flow field, we constructed a prototype of the concentric tube type firebrand generator (Fig. 2(a)). The prototype is made of 3.6 m long PVC tubes, using two tubes of nominal inner diameters (D_{ID}) 50 and 100 mm, and of lengths 1.6 and 2.9 m respectively. The prototype is constructed from the design which preliminary simulation indicated a uniform flow profile at the mouth. A 1.5 kW centrifugal fan running at 2950 rpm supplies air (Fig. 2(a)) to create suction at the firebrand inlet location which draws the firebrand through the generator. The centre line stream wise velocity at the mouth of the generator is 29.5 m/s, and the approximate particle velocity at the mouth of the generator is 12 m/s. The non-burning firebrands are fed into the firebrand generator at firebrand inlet location (Fig. 2(a)) by means of a conveyor belt. The maximum number of cubiform firebrands of 10 mm nominal size is 4 particles/s without causing clogging in the tube. The prototype does not use combusting firebrands due to the materials used in its construction. Flaming firebrands will be generated using the final version of the firebrand generator made of stainless steel, which is under construction following the prototype.

All simulation cases are generated by using a third-party CAD drawing software in Pyrosim to create FDS input files. The use of Pyrosim simplifies the generation of complicated geometries of the systems that are simulated. The tube walls have no-slip conditions with constant pressure open boundary conditions at x = 0, 4 m, y = −0.2, 0.3 m, and z = 0.6, 1.2 m with a grid of Δx 0 = Δy = Δz = 10 mm. The simulation case is compared with the experimental observations. The flow profile at the mouth of the prototype was measured using a pitot tube of 3 mm diameter (d_p) data were acquired using a Key insight 34972A at a rate of 20 scans/s for 120 s. To obtain an accurate measurement from the pitot tube corrections are applied to the measured data to accommodate the viscous, the shear, and the near-wall effects [31]. The viscous correction is not applicable as the pitot tube Reynolds number (based on local mean velocity and pitot tube diameter) is $Re_{dp} > 100$ for our prototype. The shear correction which is caused due to the non-linear averaging of the pressure variation across the probe face and asymmetric streamline deflection. This correction is applied as a virtual shift (Δy) at the location of measurement (y) towards the higher velocity direction. It is defined by Eq. (3):

$$\Delta y = \epsilon d_p \quad (3)$$

MacMillan [32] proposed a constant value of ϵ=0.15 for this correction.

The measured average velocity (U_{meas}) in the pitot tube is slightly higher than the actual average velocity (U_{act}) due to fluctuation [31], and hence, the actual average velocity is defined as

$$U_{act.} \approx \sqrt{U_{meas.}^2 - u'^2},$$

where, u' = velocity fluctuation (4)

Then the near-wall correction is applied to compensate the blockage effect of the solid boundary in the vicinity of pitot tube which reduces the shear induce stream-lines deflection. The near-wall correction is applied to the measurement points carried out at $y < 2d_p$.

$$\frac{\Delta U}{U_{act.}} = 0.015e^{-3.5\left(\frac{y}{d_p}-0.5\right)}, \text{ for } 30<d^+<230 \quad (5)$$

$$d^+ = \frac{d_p u_\tau}{\nu},$$

where, u_τ = Frictional velocity, and ν = kinematic viscosity (6)

Bailey et al. [30] suggested a modified form of MacMillan near-wall correction (Eq. (5)). The modified form is equivalent to Eq. (5), when $d^+ > 50$ and in our case we observe d^+~140. Hence, Eq. (5) is used for near-wall correction to obtain an accurate measurement by the pitot tube. Apart from these, uncertainties exist related to ambient temperature (± 1 °C), humidity (± 5%) and dynamic viscosity, which accounts for uncertainty in measurements of approximately 0.2%, 0.3% and 0.2% respectively.

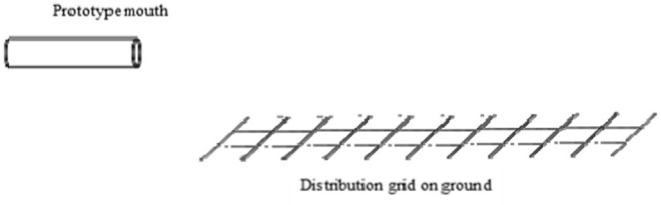

Fig. 3. Experimental rig to measure particle distribution from the prototype.

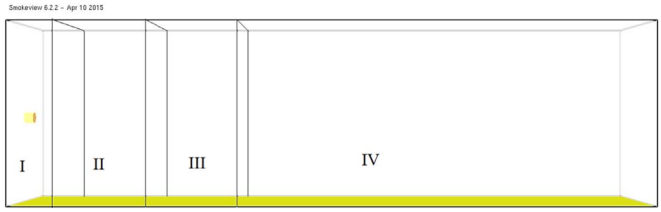

Fig. 4. Simulation domain divided into four zones to simulate particle scattering.

The mean flow contour shows a uniform flow developed at the mouth of the prototype *(Re ≈ 19200)* shown in Fig. 2(b) and (c) for XZ and XY plane. The operational Reynolds number of our generator is almost twice that of the NIST Firebrand dragon due to different flow speed and diameter of the pipe. A high velocity is observed at x = 1.1 m and z = 1 m in Fig. 2(b), which is due to flow coming from the fan tube to the concentric tubes. A comparison between the experimentally and simulated flow profiles in the X direction varied along both Y and Z axes shown in Fig. 2(d), the differences between the simulated and experimental observation near the edges are due to the effect of simulation grid resolution. Grid sensitivity analysis is carried out at three cubiform mesh sizes of 5, 10, and 15 mm, shown in Fig (e) for flow profile varying along the Z- axis and justifies the use of 10 mm cubiform grid size. The results observed are comparable to the observations made for horizontal tube by Lun and Liu [33], and Tsuji et al. [34].

4. Experimental study of particle distribution

Scattering of non-burning short-range firebrands is carried out using the aforementioned prototype. Fig. 3 shows a design layout of the experimental rig used for the experimental and simulation study. Two shapes of firebrands particles (cubiform and cylindrical) are used to study the transport of nuts, seeds, twigs, and a small chunk of bark. The cubiform particles of average size of 12.45 mm, and mass of 0.83 g (0.12 g std. dev.), and cylindrical particles of average length 11.6 mm, diameter 6.2 mm, and mass of 0.17 g (0.01 g std. dev.) are injected at a rate of 0.33 particles/s. Filkov et al. [33] and Manzello et al. [34] observed firebrand with a similar particle size range. The mass of our firebrands are on the upper extremes observed. Filkov et al. [33] measured extinguished firebrands, which will have significantly less mass than when the firebrand is initially released. The particle velocities studied here typically do not exceed 12 m/s, which is consistent with Filkov et al. [33]. Therefore, our experimental study, while lying in a realistic range, is probably at the upper end of Reynolds number that could be expected in a typical wildfire. The larger particle size in this experimental study was determined by what could easily measured by the videography. The high fluid, and hence particle, velocity near the mouth of the generator is due to the use of a jet flow, rather than the lower velocities that would be expected in the atmospheric surface layer. As the fluid jet dissipates the particle Reynolds number (Re_D) decreases significantly from ~11,000 to ~4000 into the regime observed by Filkov et al. [33].

This rate of injection ensures that the particles travel in the uniform flow field and causes minimal disturbance to flow field such that the particles can be approximated as Lagrangian particles. Particle image velocimetry (PIV) is used to estimate the particle velocity at the mouth of the prototype. The distribution of particles on the ground is carried out using videography at 720p and 120 fps to estimate the first impact on the ground. After the initial impact, the particles bounce on the ground and where they finally land depends on the physical characteristics of the surface. Hence, the final distribution is not considered. To ensure a proper distribution is achieved and experimental fluctuation are ensemble averaged and are repeated till it satisfies the following criteria defined by Eqs. (7) and (8).

$$P_i(x, y) = \frac{\sum_{i=1}^{N} (f_i(x, y)/i)}{\int_{y_l}^{y_u}\int_{x_l}^{x_u} f_i(x, y)\,dxdy}, \tag{7}$$

where, i = experiment number, $f_i(x,y)$ = number of particles in distribution grid x, y.

x_l, y_l, x_u, y_u = lower and upper of distribution grid x, y

$$Max\{P_{i+1}(x, y) - P_i(x, y)\} < 0.05 \tag{8}$$

Simulation of the experimental case is carried out in FDS. The inflow boundary condition at the prototype mouth is taken from the measured flow profile. At the inflow boundary, cubiform and cylindrical Lagrangian particles are injected into the flow field. The domain of the simulation is 7 m long, 1.2 m wide, and 2 m high respectively in X-, Y-, and Z- directions. The domain is sub-divided into four parts (Fig. 4), x = 0 – 0.5, 0.5 – 1.5, 1.5 – 2.5, and 2.5 – 7 m with uniform grid sizes (Δx = Δy = Δz) 10, 20, 40 and 40 mm respectively. Grid independence test is carried out using of grid sizes (mm) for four domains (Fig. 4) as [5, 10, 20, 40], [10, 20, 20, 40], and [10, 20, 40, 40]. For accurate simulation, six types ($\bar{\mu} \pm \sigma/4$, $\bar{\mu} \pm 3\sigma/4$, and $\bar{\mu} \pm 3\sigma/2$; $\bar{\mu}, \sigma$ are mean density and standard deviation of particle densities respectively) of cubiform (Fig. 5(a)) and cylindrical particles (Fig. 5(b)) are used covering the normal distribution of particles density used in experiments. The mean and standard deviation of cubiform and cylindrical particles density are 428.3, 492.9, 48.9, and 44.3 kg/m^3 respectively. Furthermore, the particles are given the mean u, v, and w velocities with a standard deviation (details are discussed in the Section 5 of manuscript).

5. Results

5.1. Experimental

The cubiform and cylindrical particles distribution and component of their velocities at the mouth are measured using a camera at 720p and 120 fps. The distribution of particles at the mouth of prototype shown in Fig. 6(a), in both Y- and Z- directions for cubiform particles. For cubiform particles in Z- direction, the distribution is slightly

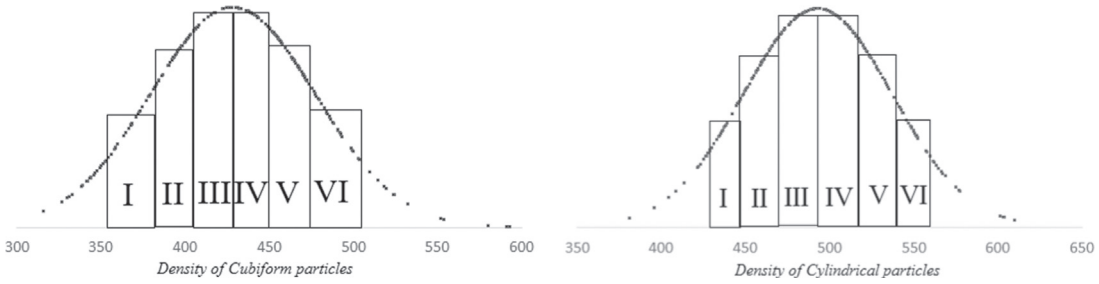

(a) Cubiform particle density distribution (b) Cylindrical particle density distribution

Fig. 5. Particle density distribution for experimental and six different types of simulated particles to cover experimental particles range.

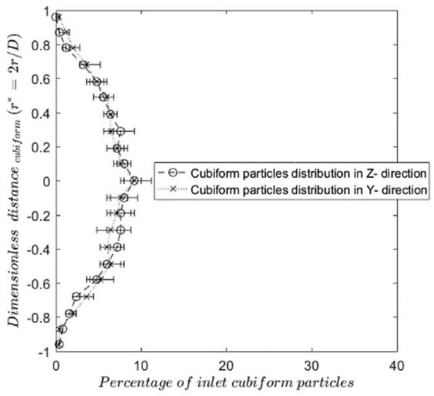

(a) Distribution of cubiform particles at the mouth of prototype

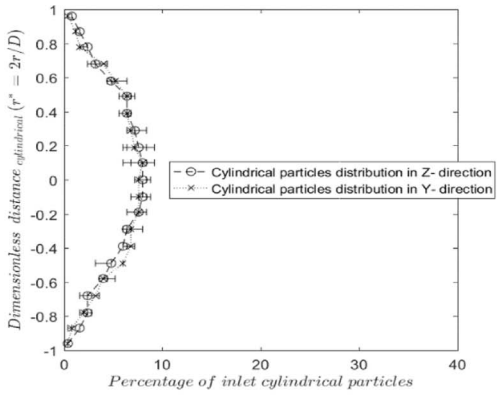

(b) Distribution of cylindrical particles at the mouth of prototype

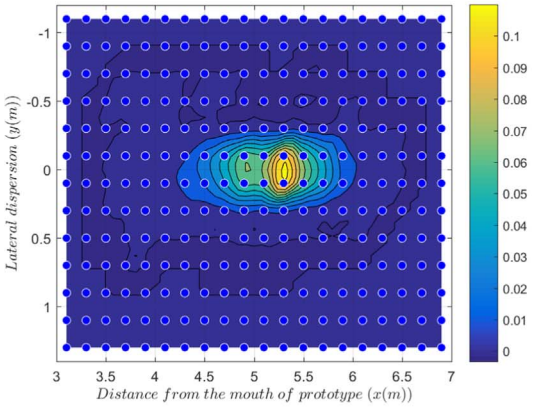

(c) Scattering of cubiform particles on the ground

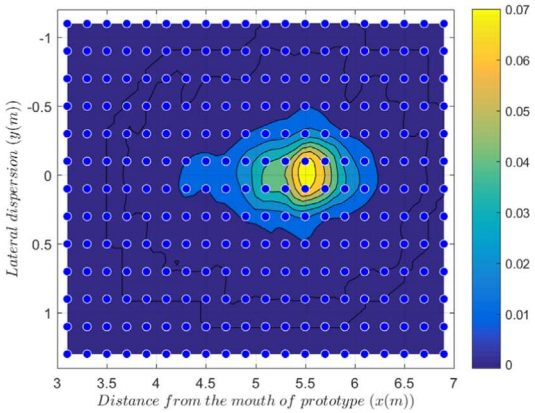

(d) Scattering of cylindrical particles on the ground

Fig. 6. Experimental distribution of cubiform and cylindrical particles at the mouth of prototype and the distribution grid on the ground.

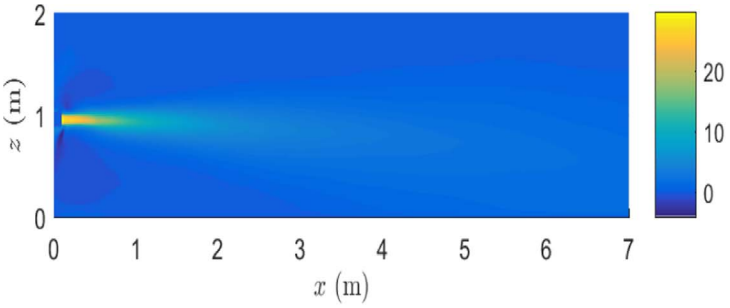

(a) Mean u- component of flow profile

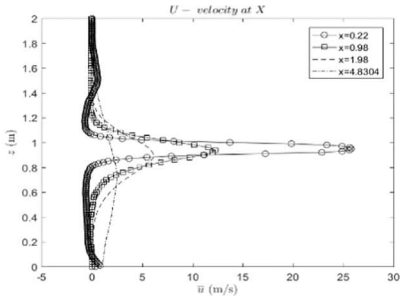

(b) u- velocity

Fig. 7. Simulation of the experimental rig.

skewed towards bottom half due to the weight of the particles. Similarly, the distribution of cylindrical particles at the mouth of prototype is shown in Fig. 6(b) in both Y- and Z- directions. The distribution of particles assume a normal distribution due to very low rate of mass loading contrast to the previous study on diluted particle flow in the horizontal tube [35,36]. The particle component velocities (u,v, and w) were estimated using PIV by measuring the displacement of the centroid of a particle streak in two directions [37]. The measured component velocities for cubiform particles are 12.5, 0.0, 0.0 m/s respectively, with standard deviations of 0.8, 0.6 and 0.6 m/s respectively. While, the measured component velocities for cylindrical particles are 13.4, 0.2, 0.2 m/s respectively, with standard deviations of 0.9, 0.7 and 0.8 m/s respectively.

Fig. 6(c) shows the average normalised contour plot of experimental runs showing the percentage of cubiform particle scatters on the distribution grid on the ground from the firebrand generator mouth. The distribution of the cubiform particle is almost a Gaussian distribution with a peak concentration of particle ~5.4 m from the mouth of the prototype. A similar distribution of cylindrical particles is presented in Fig. 6(d), however, the distribution of cylindrical particles is slightly skewed (Fig. 6(d)) with a peak concentration of particle ~5.5 m which would be the result of particles collision with the inner surface of the prototype.

The spread of cubiform particles in the Y- direction is limited due to almost uniform drag effect while there is a significant spread of cylindrical particles due to non-uniform drag effects on the particles.

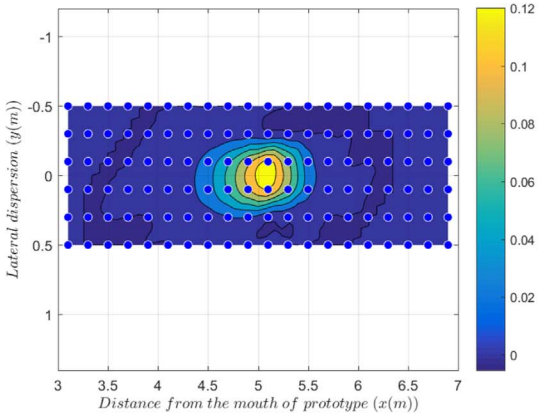

(a) Simulated scattering of cubiform particles

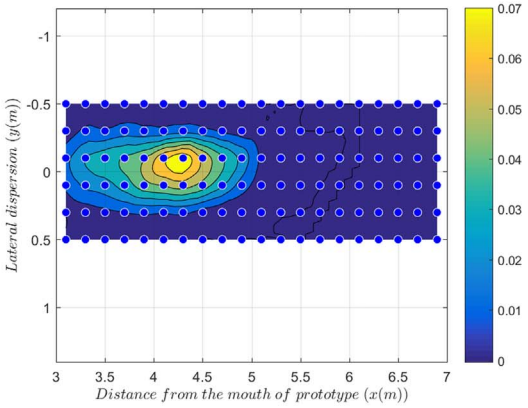

(b) Simulated scattering of cylindrical particles

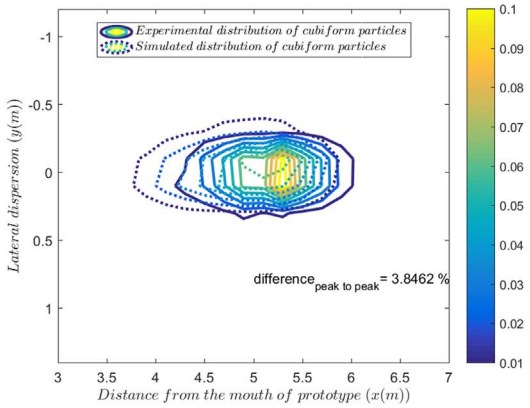

(c) Spatial comparison between experimental and simulated cubiform particles

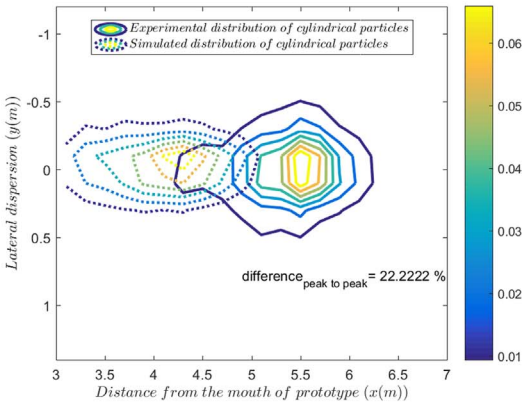

(d) Spatial comparison between experimental and simulated cylindrical particles

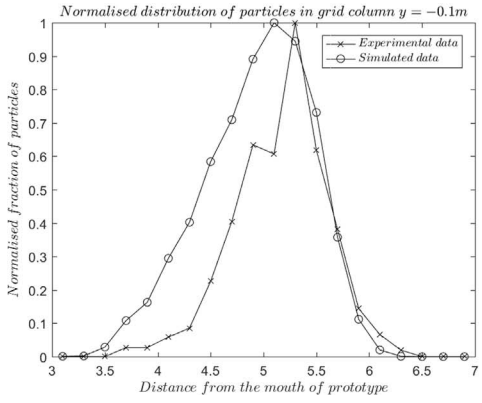

(e) Comparison between experimental and simulation at y=-0.1 m for cubiform particles

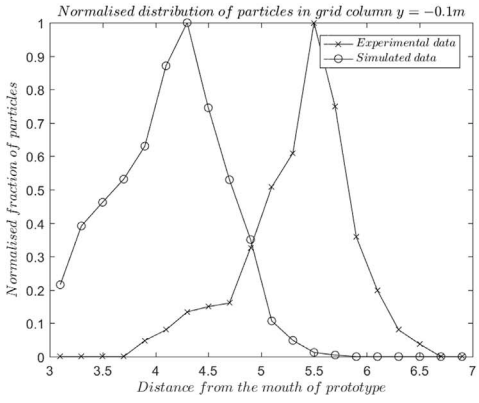

(f) Comparison between experimental and simulation at y=-0.1 m for cylindrical particles

Fig. 8. Simulated and comparative observation of cubiform and cylindrical particle scattering.

This suggests that cylindrical particles scatter more in the lateral (Y-) direction than cubiform particles for same nominal length.

5.2. Simulation

Simulation of the experimental rig is carried out in FDS, Fig. 7(a) shows the mean u- component of velocity coming from the prototype mouth. There is a strong presence of a jet until approximately 2 m from the mouth. Further, we can see a negative value of u-velocity near the edge of the mouth in Fig. 7(a) at x = 0.2 m, which is more clearly visible in Fig. 7(b) at x = 0.22 m. The negative velocity is a result of eddies formation due to shear instability near the edge of the mouth.

Fig. 8(a) and (b) shows the normalised simulated scattering of cubiform and cylindrical particles, the fraction of the particle falling near the peak area in the simulation is slightly higher than the fraction of particles falling during the experiments (Fig. 4(a) and (b)). The peaks of the distributions of particles observed is ~5.1 and ~4.3 m for cubiform and cylindrical particles respectively, which is less than the experimental observations. In the case of cylindrical particles, the distribution is under-predicted compared to the experimental observation (Fig. 8(c) & (d)), while, the observation for cubiform particles compares favourably with the experimental data. The difference in

peak to peak location for the two observations (experimental and simulated) is calculated as a relative difference in between the two peak distances from the mouth of the prototype. Underprediction of the scattering distribution, particularly in the cylindrical case is likely due to the variation in the drag coefficient caused by the tumbling of the particles. The drag coefficients used, assume that the orientation of the particle is fixed relative to the flow which is not realistic for non-spherical particles which follow a complicated trajectory. Fig. 8(e) and (f) shows an approximately Gaussian distribution of particles observed in experiment and simulation in a column of particle distribution grid. This Gaussian distribution is quite similar to the one seen in the literature [15,38] for cylindrical particles.

6. Conclusions

A new prototype firebrand dragon is shown to successfully generate uniform showers of firebrands. The prototype is useful to study the transport dynamics of short-range firebrand transport. The Lagrangian particle model of FDS is capable of simulating the transport of non-burning solid firebrand particles with reasonable accuracy. The model is verified for two shapes of firebrand particles; the results are under-predicted compared to experimental observations. Application of the Lagrangian model for flaming firebrands and improvement of default FDS Lagrangian models will be the next step to evaluate the applicability of the model for short-range firebrand transport.

Acknowledgement

We wish to acknowledge the financial support given by Bushfire and Natural Hazard Cooperative Research Centre (BNHCRC), Melbourne, Australia. The authors wish to thank Mr Lyndon Macindoe and Mr Philip Dunn for their support in constructing the firebrand generator prototype at Victoria University. Also, authors wish to thank the administrative team of the Edward HPC, University of Melbourne for their support in running of simulations.

References

[1] C. Stephenson, J. Handmer, A. Haywood Estimating the net cost of the 2009 Black Saturday Fires to the affected regions, 2012.
[2] S.L. Manzello, S. Suzuki, Experimentally simulating wind driven firebrand showers in wildland-urban interface (WUI) fires: overview of the NIST firebrand generator (NIST dragon) technology, Procedia Eng. 62 (2013) 91–102. http://dx.doi.org/10.1016/j.proeng.2013.08.047.
[3] V.C. Radeloff, R.B. Hammer, S.I. Stewart, J.S. Fried, S.S. Holcomb, J.F. McKeefry, The Wildland-Urban Interface in the United States, Ecol. Appl. 15 (2005) 799–805.
[4] A.L. Sullivan, Wildland surface fire spread modelling, 1990–2007. 1: physical and quasi-physical models, Int. J. Wildland Fire 18 (2009) 349–368. http://dx.doi.org/10.1071/WF06144.
[5] A.L. Sullivan, Wildland surface fire spread modelling, 1990–2007. 2: empirical and quasi-empirical models, Int. J. Wildland Fire 18 (2009) 369–386. http://dx.doi.org/10.1071/WF06142.
[6] A.L. Sullivan, Wildland surface fire spread modelling, 1990–2007. 3: simulation and mathematical analogue models, Int. J. Wildland Fire 18 (2009) 387–403. http://dx.doi.org/10.1071/WF06144.
[7] R. Blanchi, J. Leonard, R.H. Leicester, Bushfire Risk at the Rural/UrbanInterface, Australasian Bushfire Conference, 2006.
[8] M.G. Cruz, A.L. Sullivan, J.S. Gould, N.C. Sims, A.J. Bannister, J.J. Hollis, R.J. Hurley, Anatomy of a catastrophic wildfire: the Black Saturday Kilmore East fire in Victoria, Australia, For. Ecol. Manag. 284 (2012) 269–285. http://dx.doi.org/10.1016/j.foreco.2012.02.035.
[9] M.G. Cruz, J.S. Gould, M.E. Alexander, A.L. Sullivan, W.L. McCaw, S. Mathews, A Guide to Rate of Fire Spread Models for Australian Vegetation, CSIRO Land and Water Flagship, Canberra, ACT and AFAC, Melbourne, VIC, 2015.
[10] P.F. Ellis, The Aerodynamic and Combustion Characteristics of Eucalypt Bark – A Firebrand Study (PhD thesis), Australian National University, Canberra, Australia, 2000.
[11] P.F.M. Ellis, The likelihood of ignition of dry-eucalypt forest litter by firebrands, Int. J. Wildland Fire 24 (2015) 225–235. http://dx.doi.org/10.1071/WF14048.
[12] D.M. Chong, K.G. Tolhurst, T.J. Duff, Incorporating Vertical Winds into PHOENIX RapidFire's Ember Dispersal Model, Technical Report, Bushfire CRC/University of Melbourne, 2012.
[13] P.F.M. Ellis, A Review of Empirical Studies of Firebrand Behaviour, Bushfire Cooperative Research Centre (CRC), Melbourne, Australia, 2012.
[14] A. Tohidi, N. Kaye, W. Bridges, Statistical description of firebrand size and shape distribution from coniferous trees for use in Metropolis Monte Carlo simulations of firebrand flight distance, Fire Saf. J. 77 (2015) 21–35. http://dx.doi.org/10.1016/j.firesaf.2015.07.008.
[15] S.L. Manzello, J.R. Shields, T.G. Cleary, A. Maranghides, W.E. Mell, J.C. Yang, Y. Hayashi, D. Nii, T. Kurita, On the development and characterization of a firebrand generator, Fire Saf. J. 43 (2008) 258–268. http://dx.doi.org/10.1016/j.firesaf.2007.10.001.
[16] S.L. Manzello, S. Suzuki, D. Nii, Full-scale Experimental investigation to quantify building component ignition vulnerability from mulch beds attacked by firebrand showers, Fire Technol. (2015) 1–17. http://dx.doi.org/10.1007/s10694-015-0537-3.
[17] S.L. Manzello, S. Suzuki, Y. Hayashi, Enabling the study of structure vulnerabilities to ignition from wind driven firebrand showers: a summary of experimental results, Fire Saf. J. 54 (2012) 181–196. http://dx.doi.org/10.1016/j.firesaf.2012.06.012.
[18] K. Zhou, S. Suzuki, S.L. Manzello, Experimental study of firebrand transport, Fire Technol. 51 (2014) 785–799. http://dx.doi.org/10.1007/s10694-014-0411-8.
[19] W. Mell, M.A. Jenkins, J. Gould, P. Cheney, A physics-based approach to modelling grassland fires, Int. J. Wildland Fire 16 (2007) 1–22. http://dx.doi.org/10.1071/WF06002.
[20] W. Mell, A. Maranghides, R. McDermott, S.L. Manzello, Numerical simulation and experiments of burning douglas fir trees, Combust. Flame 156 (2009) 2023–2041. http://dx.doi.org/10.1016/j.combustflame.2009.06.015.
[21] T. Sikanen, J. Vaari, S. Hostikka, A. Paajanen, Modeling and simulation of high pressure water mist systems, Fire Technol. 50 (2014) 483–504. http://dx.doi.org/10.1007/s10694-013-0335-8.
[22] H.M.I. Mahmud, K.A.M. Moinuddin, G.R. Thorpe, Study of water-mist behaviour in hot air induced by a room fire: model development, validation and verification, Fire Mater. 40 (2016) 190–205. http://dx.doi.org/10.1002/fam.2279.
[23] H.M.I. Mahmud, K.A.M. Moinuddin, G.R. Thorpe, Experimental and numerical study of high-pressure water-mist nozzle sprays, Fire Saf. J. 81 (2016) 109–117. http://dx.doi.org/10.1016/j.firesaf.2016.01.015.
[24] R.J. McDermott, G.P. Forney, K. McGrattan, W.E. Mell Fire Dynamic Simulator 6: Complex geometry, embedded meshes, and quality assessment, V European Conference on Computational Fluid Dynamic, ECCOMAS CFD 2010, Lisbon, Portugal, 2010.
[25] K. McGrattan, S. Hostikka, J. Floyd, R. McDermott, C. Weinschenk, K. Overholt, Fire Dynamics Simulator Technical Reference Guide Volume 1: Mathematical Model, National Institute of Standards and Technology, Special Publication 1018, Gaithersburg, MD, 2013, p. 149.
[26] W.R. Dean, XVI. Note on the motion of fluid in a curved pipe, Lond. Edinb. Dublin Philos. Mag. J. Sci. 4 (1927) 208–223. http://dx.doi.org/10.1080/14786440708564324.
[27] R. Röhrig, S. Jakirlić, C. Tropea, Comparative computational study of turbulent flow in a 90° pipe elbow, Int. J. Heat Fluid Flow 55 (2015) 120–131. http://dx.doi.org/10.1016/j.ijheatfluidflow.2015.07.011.
[28] K.W. Chu, A.B. Yu, Numerical simulation of complex particle-fluid flows, Powder Technol. 179 (2008) 104–114. http://dx.doi.org/10.1016/j.powtec.2007.06.017.
[29] K. Mohanarangam, Z.F. Tian, J.Y. Tu, Numerical simulation of turbulent gas-particle flow in a 90° bend: Eulerian-Eulerian approach, Comput. Chem. Eng. 32 (2008) 561–571. http://dx.doi.org/10.1016/j.compchemeng.2007.04.001.
[30] K. Sun, L. Lu, H. Jiang, A computational investigation of particle distribution and deposition in a 90° bend incorporating a particle-wall model, Build. Environ. 46 (2011) 1251–1262. http://dx.doi.org/10.1016/j.buildenv.2010.12.006.
[31] S.C.C. Bailey, M. Hultmark, J.P. Monty, P.H. Alfredsson, M.S. Chong, R.D. Duncan, J.H.M. Fransson, N. Hutchins, I. Marusic, B.J. McKeon, H.M. Nagib, R. Orlü, A. Segalini, A.J. Smits, R. Vinuesa, Obtaining accurate mean velocity measurements in high Reynolds number turbulent boundary layers using Pitot tubes, J. Fluid Mech. 715 (2013) 642–670. http://dx.doi.org/10.1017/jfm.2012.538.
[32] F.A. MacMillan, Experiments on Pitot tubes in shear flow, vol. 3028, HM Stationery Office, 1957.
[33] A. Filkov, S. Prohanov, E. Mueller, D. Kasymov, P. Martynov, M. El Houssami, J. Thomas, N. Skowronski, B. Butler, M. Gallagher, K. Clark, W. Mell, R. Kremens, R.M. Hadden, A. Simeoni, Investigation of firebrand production during prescribed fires conducted in a pine forest, Proc. Combust. Inst. 36 (2016) 1–8. http://dx.doi.org/10.1016/j.proci.2016.06.125.
[34] S.L. Manzello, A. Maranghides, W.E. Mell, Firebrand generation from burning vegetation, Int. J. Wildland Fire 16 (2007) 458–462. http://dx.doi.org/10.1071/WF06079.
[35] C.K.K. Lun, H.S. Liu, Numerical simulation of dilute turbulent gas-solid flows in horizontal channels, Int. J. Multiph. Flow 23 (1997) 575–605. http://dx.doi.org/10.1016/S0301-9322(96)00087-0.
[36] Y. Tsuji, Y. Morikawa, T. Tanaka, N. Nakatsukasa, M. Nakatani, Numerical simulation of gas-solid two-phase flow in a two-dimensional horizontal channel, Int. J. Multiph. Flow 13 (1987) 671–684. http://dx.doi.org/10.1016/0301-9322(87)90044-9.
[37] J. Westerweel, Fundamentals of digital particle image velocimetry, Meas. Sci. Technol. 8 (1997) 1379–1392. http://dx.doi.org/10.1088/0957-0233/8/12/002.
[38] Y.D. Kim, Y. Hayashi, C.Y.J. Tri, S.J. Baek A numerical study on travel distances of firebrands by wind, in: Proceedings of the 7th Asia-Pacific Conference on Wind Engineering, APCWE-VII, November 8, 2009–November 12, 2009.